Single-cell RNA sequencing of peripheral blood mononuclear cells in patients with acutely decompensated cirrhosis reveals a specific monocyte subset associated with an increased risk of progression to ACLF

Authors:

Theresa H. Wirtz[1†], Sara Palomino-Echeverria[2,3,4†*], Maike R. Pollmanns[1], Estefanía Huergo[2], Felix Schreibing[5], Johanna Reißing[1], Cristina Sánchez-Garrido[6], Cristina López-Vicario[6,7,8], Ana M. Aransay[8,9], Maurizio Baldassare[10], Giacomo Zaccherini[10,11], Enrico Pompili[10,11], Martin Schulz[12], Frank E. Uschner[12], Sabine Klein[12], Wenyi Gu[12], Robert Schierwagen[12], Shantha Valainathan[13], Annabelle Verbeeck[13], Daniela Campion[14], Ilaria Giovo[14], Alexander Koch[1], Rafael Kramann[5,15], Tony Bruns[1], Narsis Kiani[16], Paolo Caraceni[10,17], Carlo Alessandria[14], Richard Moreau[6,13,18], Jonel Trebicka[6,12], Joan Clària[6,7,8,19], Núria Planell[20*], Pierre-Emmanuel Rautou[6,13,18#*], Christian Trautwein[1,21,22#*], David Gomez-Cabrero[2,23#*]

Affiliations:

[1]Medical Department III, University Hospital RWTH Aachen, Aachen, Germany
[2]Translational Bioinformatics Unit (TransBio), Navarrabiomed, Navarra Health Department (CHN), Public University of Navarra (UPNA), Navarra Institute for Health Research (IdiSNA), Pamplona, Spain
[3]Research Program in Systems Oncology, University of Helsinki, Helsinki, Finland
[4]Institute for Molecular Medicine Finland, Helsinki Institute for Life Sciences, University of Helsinki, Helsinki, Finland
[5]Department of Medicine 2 (Nephrology, Rheumatology, Clinical Immunology and Hypertension), RWTH Aachen University, Medical Faculty, Aachen, Germany
[6]European Foundation for the Study of Chronic Liver Failure (EF CLIF) and Grifols Chair, Barcelona, Spain
[7]Biochemistry and Molecular Genetics Service, Hospital Clinic-IDIBAPS, Barcelona, Spain
[8]CIBERehd, Madrid, Spain
[9]Center for Cooperative Research in Biosciences (CIC bioGUNE), Derio, Bizkaia, Spain
[10]Unit of Semeiotics, Liver and Alcohol-related Diseases, IRCCS Azienda Ospedaliero-Universitaria di Bologna, Bologna, Italy
[11]Department of Medical and Surgical Sciences (DIMEC), Alma Mater Studiorum, University of Bologna, Bologna, Italy
[12]Department of Internal Medicine B, University Hospital Muenster, Muenster, Germany
[13]AP-HP, Hôpital Beaujon, Service d´Hepatologie, DMU DIGEST, Centre de Référence des Maladies Vasculaires du Foie, FILFOIE, ERN RARE-LIVER, Clichy, France
[14]Division of Gastroenterology and Hepatology, A.O.U. Città della Salute e della Scienza di Torino, Torino, Italy
[15]Department of Internal Medicine, Nephrology and Transplantation, Erasmus Medical Center, Rotterdam, The Netherlands
[16]Algorithmic Dynamics lab, Department of Oncology-Pathology, Karolinska Institutet, Solna, Sweden
[17]IRCCS Azienda Ospedaliera-Universitaria di Bologna, Bologna, Italy
[18]Université Paris-Cité, Inserm, Centre de recherche sur l´inflammation, UMR 1149, Paris, France
[19]Department of Biomedical Sciences, University of Barcelona, Spain
[20]Universidad de Navarra, Centro de Investigación Médica Aplicada (CIMA), Computational Biology Program, Instituto de Investigación Sanitaria de Navarra (IdiSNA), Pamplona, Spain
[21]Leibniz Research Centre for Working Environment and Human Factors at the TU Dortmund (IfADo), Dortmund, Germany
[22]Liver Center, Department of Gastroenterology, Hepatology and GI-Oncology, Klinikum Stuttgart, Stuttgart, Germany
[23]Bioscience Program, Biological and Environmental Sciences and Engineering Division (BESE), King Abdullah University of Science and Technology KAUST, Thuwal, Saudi Arabia

†: These authors contributed equally to this work and share first authorship. Either name may be listed first when citing.
#: These authors contributed equally to this work and share last authorship.
*: **Corresponding authors:** sara.palominoecheverria@helsinki.fi, nplanellpic@unav.es, pierre-emmanuel.rautou@inserm.fr, trautwein.christian@gmx.net, david.gomez.cabrero@navarra.es

Key words: acute decompensation, acute-on-chronic liver failure, cirrhosis, prognosis, scRNA-seq, CITE-seq, monocytes, CD14, energy metabolism

Abstract

Background: Patients with acute decompensation (AD) of cirrhosis are at high risk of developing acute-on-chronic liver failure (ACLF), a syndrome characterized by multiple organ failure and high short-term mortality. This study aimed to analyse alterations in peripheral blood mononuclear cells (PBMCs) in patients with AD using single-cell technologies and to explore their implications for risk stratification and prognosis.

Methods: A total of 63 AD patients and 15 healthy donors were enrolled at five European centers, with blood samples collected upon hospital admission. Patients were monitored for 90 days after study inclusion, focusing on hospital readmission related to AD and the development of ACLF. Cellular indexing of transcriptomes and epitopes by sequencing (CITE-seq) was performed on PBMCs from 16 patients (n=6 without readmission, n=6 with readmission, and n=4 with ACLF development) along with 4 healthy controls. The whole blood of the same 16 patients was assessed by bulk RNA-seq. The whole blood transcriptional profiles from two independent prospective multicentre cohorts of patients with AD (PREDICT (n=689) and ACLARA (n=521)) were included as validation cohorts.

Results: Cell proportion analysis revealed a significant increase of classical monocytes in patients with subsequent ACLF development. Notably, classical monocytes represented the cell type with the highest transcriptional alterations. Within the classical monocyte population, a specific subcluster, termed “C2”, was identified and found to be enriched during progression towards ACLF. This monocytic subpopulation was primarily characterized by decreased expression of genes encoding enzymes relevant to cellular energy supply, such as oxidative phosphorylation and ATP production. Pathway analysis confirmed a marked impairment of energy metabolism pathways within the C2 subcluster. A gene signature derived from that monocytic subpopulation was significantly increased in patients with bacterial infection, ACLF development and non-survivors of two independent multicenter cohorts of patients with AD.

Conclusion: Patients with acute decompensation of cirrhosis who subsequently develop ACLF are characterized by a subpopulation of classical monocytes exhibiting features of impaired energy metabolism pathways.

Introduction

Acute decompensation (AD) is the most frequent cause of hospitalization among individuals diagnosed with cirrhosis (1). It involves the emergence of one or more clinically relevant complications, such as ascites, hepatic encephalopathy, or gastrointestinal bleeding (2–4). Patients with AD are at high risk of developing acute-on-chronic liver failure (ACLF) – a clinical syndrome marked by the acute deterioration of liver function in individuals with AD accompanied by the failure of one or more major organs or systems (5,6). Depending on the severity and number of organ failures, ACLF is associated with poor short-term mortality ranging from 15% to 80% (7).

The transition from decompensated cirrhosis to ACLF is a dynamic and multifactorial process driven by a complex interplay of systemic inflammation (SI), immune dysfunction, and organ crosstalk (8,9). Significant progress has been made in understanding the underlying pathophysiological mechanisms as well as identifying the pivotal mediators that initiate and regulate these processes. Particularly, SI was identified to gradually increase with the progression of portal hypertension and to induce organ dysfunction as part of ACLF transition (10,11). Respective studies have identified increased circulating levels of pro-inflammatory cytokines and the activation of innate immune pathways, including Toll-like receptor (TLR) signaling, as key contributors (12,13). Furthermore, the translocation of microbial products from the gut into systemic circulation, a consequence of intestinal barrier dysfunction, has been implicated in exacerbating SI and immune activation (14). In parallel, cellular studies have revealed immune cells to exhibit phenotypic and functional alterations that promote SI and impair immune response. Dysfunctional neutrophils and monocytes have been identified to impair innate immunity and increase susceptibility to bacterial infection – a common trigger of ACLF (15–17).

Despite these advances, the relative contributions of different immune cell subsets during disease progression are incompletely defined, and the identification of functional cellular states associated with ACLF development remains an area of investigation. Single-cell technologies, including single-cell RNA sequencing (scRNA-seq), have emerged as transformative tools for dissecting cellular heterogeneity and capturing the dynamic immune landscape in complex diseases. Hence, recent studies have used scRNA-seq to elucidate pathophysiological characteristics of peripheral immune cells in patients with ACLF compared to healthy controls (18–21). They identified distinct immunometabolic cellular states contributing to ACLF outcome, with the most significant changes in pro-inflammatory monocytes and T-cells (18–21). However, those publications focused on patients who already transitioned to ACLF. Yet, no prospective, high-resolution baseline analysis of functional alterations of peripheral immune cells in patients with AD who subsequently develop ACLF is available.

We, therefore, conducted a prospective multicenter study involving patients admitted due to AD at five different European centers. The aim of the study was to characterize the PBMCs at single-cell resolution. Our data provide insights into changes within peripheral immune cell subpopulations associated with AD progression, as well as molecular mechanisms driving ACLF development.

113 ## Material and Methods

114 *Study design*

115 A prospective multicenter study was conducted in 5 European centers (Hôpital Beaujon, Université
116 Paris-Cité, France; Goethe University Frankfurt, Germany; RWTH Aachen University, Germany;
117 University of Bologna, Italy; University of Turin, Italy) between October 2020 and July 2021. Patients
118 who were admitted to the hospital due to AD (ascites, overt hepatic encephalopathy, new onset of
119 non-obstructive jaundice, gastrointestinal hemorrhage, and/or bacterial infections) met the inclusion
120 criterion and were screened for exclusion criteria (**Supplementary Table 1**). A total of 63 patients with
121 AD and 15 healthy controls were recruited. Written informed consent was obtained from the patient,
122 her/his spouse, or the appointed legal guardian upon hospital admission. Clinical data were collected,
123 and sample acquisition was performed within 72 hours after hospital admission in all included
124 patients. Patients were followed up for 90 days, and readmission due to AD, development of ACLF,
125 and outcome were documented (for detailed study design and visit schedule, **Supplementary Figure**
126 **1** and **Supplementary Table 2**). The study protocol was approved by the local ethics committee of
127 each participating center (Paris, Frankfurt, Aachen, Bologna, Turin) and conducted in accordance with
128 the Declaration of Helsinki.
129

130 *Sample collection and PBMC isolation*

131 After study inclusion, peripheral blood was drawn from all participants from the *discovery* cohort,
132 using BD vacutainer CPT tubes (BD Biosciences; (22)) for PBMC isolation and TempusTM tubes (Applied
133 Biosystems) for whole blood assessment. After density gradient centrifugation at 1500 RCF for 20
134 minutes at 20°C PBMCs were aspirated and then cryopreserved using fetal calf serum with 10% DMSO.
135 The cells were gradually frozen and stored at -80°C for several weeks until library preparation and
136 sequencing or flow cytometry analysis, respectively.

137 *Group allocation and patient selection strategy for single-cell analysis*

138 90 days after study inclusion, patients were classified according to their clinical course as no
139 readmission due to AD ("stable decompensated cirrhosis", SDC, n=46), readmission due to AD
140 ("unstable decompensated cirrhosis", UDC, n=8) or ACLF development within 28 days ("pre-ACLF",
141 n=10). The diagnostic criteria of ACLF were according to the EF-CLIF definition (5). Of the 63 recruited
142 patients, samples from 4 pre-ACLF, 6 UDC, and 6 SDC patients, along with four healthy controls, were
143 selected to represent the entire study cohort and subjected to CITE-seq profiling (detailed in
144 **Supplementary Material** and **Supplementary Tables 3, 4, and 5**). For baseline characteristics analysis,
145 categorical variables were summarized as counts (percentages), and continuous variables as median
146 (interquartile range, IQR). The Wilcoxon–Mann–Whitney test was used for continuous variables, and
147 the chi-square test for categorical variables.

148 *CITE-seq*

149 *Library preparation, sequencing, and demultiplexing*

150 The isolated PBMCs were recovered by gently thawing and immediately diluting in pure FCS. Next,
151 cells were centrifuged at 500 RCF for 7 minutes at 20°C, and the supernatant was removed. PBMCs
152 were then resuspended in 4 ml 5% FCS in PBS and filtered through a 20 µm pluriStrainer® provided by
153 pluriSelect (Leipzig, Germany) to obtain a single-cell solution. After the PBMCs were passed through a
154 strainer, a second centrifugation was performed. The supernatant was removed, and cells were

155 diluted in 100 µl 5% FCS in PBS. 5 µl Human TruStain FcX (BioLegend) was added and incubated for 10
156 minutes at 4°C.

157 A panel of 23 TotalSeq-C antibodies (BioLegend) was pooled, using 0.5 µg of each antibody
158 (**Supplementary Table 6**). Samples were incubated with the TotalSeq-C antibody pool for 30 min at
159 4°C. Cells were washed two times using 3 ml 5% FCS in PBS and rediluted in 1.5 ml of sorting buffer
160 (5% FCS in PBS).

161 For the detection of dead cells, DAPI was added at a final concentration of 0.5 µg/ml. Up to 300,000
162 cells from each sample were sorted on a Sony Cell Sorter by life/dead sorting. Sorted viable cells were
163 resuspended in 10 µl 1% BSA in PBS, counted, and ~20,000 cells in 38.7 µl were applied to single cell
164 partitioning and barcoding *via* Chromium Controller (10x Genomics).

165 Each participant's sample was prepared into two distinct libraries: (I) 5' Gene Expression Library (GEX),
166 designed for scRNA-seq to capture transcriptome data; and (II) Surface Protein Library, which utilized
167 TotalSeq-C barcodes to profile surface proteins, aligning with the CITE-seq methodology.

168 Cell Ranger (v6.01) was used for read alignment, filtering, barcode processing, and UMI counting with
169 default settings (23). GRCh38-2020 was used as the transcriptome reference. Specifically, STAR was
170 used in FASTQs alignment (24). Cell barcodes were then automatically determined based on the
171 distribution of the UMI count.

172 *Pre-processing*

173 We used the R package *Seurat* v4.3.0 (25) to preprocess the gene-barcode matrix and the surface
174 protein matrix of both patients and healthy controls and to perform further analysis. For each sample,
175 genes not observed in at least three cells were dropped. Low-quality or damaged cells were excluded
176 using a combination of a number of expressed genes (cells with <300 and >3500 genes) and
177 mitochondrial transcript percentages (cells with >10% mitochondrial genes). Each sample dataset was
178 normalized using the *'SCTransform'* function (26) from the *Seurat* package and regression of
179 mitochondrial RNA and cell cycle genes.

180 *Integration, clustering, and cell type identification*

181 The filtered and cleaned single-cell dataset underwent a process to identify highly variable genes and
182 remove unwanted sources of variation. This was done by calculating and extracting a subset of
183 features that show high cell-to-cell variation in the dataset using the '*FindVariableFeatures'* Seurat's
184 function. Additionally, the *'FeatureScatter'* plot from *Seurat* was applied, and we removed the
185 detected outliers when plotting feature-feature relationships (27). Harmony was used to correct for
186 batch effects (28). For each sample where the protein surface markers data was available, we selected
187 the most variable protein sub-space and applied feature-wise centered log-ratio transformation (CLR)
188 (29). Data were visualized using UMAP. Data were scaled, and the dimensionality was reduced by PCA.
189 To identify cell clusters, a shared nearest neighbor (SNN) graph was built using distances in PCA space
190 (top 1 to 20 components) through Seurat's *'FindNeighbors'* function. The Louvain algorithm was then
191 employed to iteratively cluster neighboring cells using Seurat's *'FindClusters'* function, using a
192 resolution parameter of 0.5. Cell type annotation was done by combining three parallel evaluations:
193 gene expression of canonical marker genes (**Supplementary Figure 2**), surface protein markers

194 (**Supplementary Figure 3 A, B**), and Azimuth results (a reference-based approach using an external
195 well-annotated dataset of PBMCs (25)).

196 *Cluster Composition Analysis: changes in cell proportions between groups*

197 Differences in cell type proportion between conditions were assessed by comparing the proportional
198 differences in cell populations between AD patients and healthy controls for both gene expression and
199 protein surface markers data, utilizing the *'sc_utils'* function from *scProportionTest* package with
200 default parameters (30). The estimations of the p-value and the confidence interval of the magnitude
201 of the difference are computed respectively using a permutation test and bootstrapping.

202 *Differential expression analysis, pathway analysis, and trajectory analysis*

203 Seurat *'FindAllMarkers'* function with the default Wilcoxon rank sum test based on the normalized
204 data was used to identify the cluster markers used for cluster annotation. The '*FindMarkers'* function
205 was employed to identify markers for each cell cluster to measure differential gene expression
206 between conditions, using the default Wilcoxon rank sum test method. Genes detected in less than
207 50% of both evaluated groups were discarded. We considered differentially expressed genes (DEG) to
208 be statistically significant if the adjusted p-value < 0.05 (Benjamini-Hochberg (BH)) and absolute Fold
209 Change (FC) > 1.5. '*VlnPlot*', '*FeaturePlot*,' and '*Dotplot'* functions were applied to visualize gene
210 expression in each cell type or group.

211 Next, Gene Set Enrichment Analysis (GSEA) was performed using the R package *ClusterProfiler* (31),
212 considering the comprehensive functions included in Gene Ontology (GO). Biological pathways in
213 which genes appeared at a different frequency than expected were considered enriched. The results
214 were visualized using default enrichment plots. Enrichment scores with p-value adjusted < 0.05 were
215 considered significant. The differences in the pathways among patient groups were computed using
216 the non-parametric Kruskal Wallis test.

217 Single-cell trajectory analyses were computed using the *'learn_graph'* function from the *Monocle3*
218 package with default parameters (32). We then plot the cells based on their *pseudotime*.

219 *Module scores for specific gene sets*

220 We utilized cell module scores to quantify the extent of individual cell expression of specific
221 predefined gene sets. For this purpose, we used the '*AddModuleScore'* function from *Seurat* with
222 default settings. The lists of genes defining this module were prepared based on the intersection of
223 upregulated DEGs resulting from various differential expression analyses (DEA). Differences in module
224 scores were assessed using the non-parametric Kruskal Wallis test.

225 *Bulk RNA-seq*

226 *Library preparation, sequencing and demultiplexing*

227 Bulk RNA-seq was performed in collaboration with the Genomics platform of the Center for
228 Cooperative Research in Biosciences (CIC bioGUNE), Derio, Bizkaia, Spain. RNA was extracted from
229 whole blood collected in Tempus™ tubes from the *discovery* cohort using the Extraction Tempus™
230 Spin RNA Isolation Kit (Applied Biosystems). The extracted RNA was treated with DNase. RNA quality
231 was assessed using Agilent RNA 6000 Nano and Pico Chips (Agilent Technologies). RNA concentration
232 was assessed using RNA HS Assay Kit in a Qubit 2.0 fluorometer (Thermo Fisher Scientific).

233 Sequencing libraries were prepared using the NuGEN UniversalPlus mRNA-Seq with NuQuant kit
234 (Tecan Life Sciences, Cat.#0520-24) and following the user guide (M01485v6.1andv7). The kit is
235 intended to prepare sequencing libraries depleted of globin. Briefly, starting from 500 ng of total RNA,
236 rRNA, and globin mRNA were depleted, and the remaining RNA was purified, fragmented, and primed
237 for cDNA synthesis. cDNA first strand was synthesized with SuperScript-II Reverse Transcriptase
238 (Thermo Fisher Scientific, Cat.#18064-014) for 10 min at 25°C, 15 min at 42°C, 15 min at 70°C and
239 pause at 4°C. The second strand of cDNA was synthesized with Illumina reagents at 16°C for 1 hour.
240 Then, A-tailing and adaptor ligation were performed. Finally, enrichment of libraries was achieved by
241 PCR (30 s at 98°C; 15 cycles of 10 s at 98°C, 30 s at 60°C, 30 s at 72°C; 5min at 72°C and pause at 4°C).

242 Afterward, libraries were visualized on an Agilent 2100 Bioanalyzer using Agilent High Sensitivity DNA
243 kit (Agilent Technologies, Cat. # 5067-4626), quantified using Qubit dsDNA HS DNA Kit (Thermo Fisher
244 Scientific, Cat. # Q32854) and sequenced in a NovaSeq-6000 (Illumina Inc.) by at least 40 million
245 paired-end 100nt reads.

246 Raw reads were demultiplexed via bclfastq2 Conversion Software v2.20 (Illumina) to convert base call
247 (BCL) files into FastQ files. Quality control of FastQ files was performed using FastQC (Bioinformatics
248 Babraham Institute) (33), and reads were trimmed for contaminating sequence adapters and poor-
249 quality bases using Trimmomatic (34). Sequencing reads were aligned to the Human (GRCh38) genome
250 with STAR (2.6.1) setting the parameters to default values (24). Uniquely aligned reads were assigned
251 to GENCODE18 gene annotations using HTSeq v0.11 and quantified with htseq-counts run in stranded
252 mode with default parameters (35).

253 *Bulk RNA-seq downstream analysis*

254 R v4.3.0 was employed in the downstream analysis of RNA-seq data. Genes exhibiting more than 1
255 count per million (CPM) in at least three samples were selected for the analysis. Utilizing the *limma-*
256 *voom* workflow (36), RNA-seq count data was normalized, and variance estimation was performed.
257 PCA was applied to the normalized data to assess sample similarity.

258 *Module scores*

259 A module score was calculated for each evaluated sample group using the Gene Set Variation Analysis
260 (*GSVA*) R package v1.42.0 (37) in the single-cell paired bulk RNA-seq, as well as in the PREDICT and the
261 ACLARA cohorts. This gene signature was calculated using previously selected genes to compute the
262 module score at the single-cell level.

263 *Flow Cytometry Analysis*

264 Flow cytometry of peripheral $CD14^+$ monocytes was conducted. For this purpose, additional PBMC
265 aliquots from the discovery cohort were used. First, PBMCs were thawed gently, as described above.
266 Subsequently, $CD14^+$ cells were enriched by magnetic cell separation using positive selection for
267 human CD14 (Miltenyi Biotec, Bergisch Gladbach, Germany) for in vitro experiments.

268 For surface marker expression analysis, $CD14^+$ peripheral monocytes were incubated with
269 fluorochrome-conjugated primary antibodies at optimal dilutions at 4°C for 30 min in PBS containing
270 0.5% fetal calf serum and 2 mmol/L EDTA. Single-color staining, isotype-matched controls (IMCs), and
271 fluorescence minus one (FMO) controls were applied. The antibodies used were CD14 (clone HCD14),
272 CD16 (3G8), and human leukocyte antigen-DR (HLA-DR) (G46-6).

273 Cell viability was determined with the LIVE/DEAD™ Fixable Aqua Dead Cell Stain Kit from Thermo
274 Fisher and IMC mouse IgG1 κ and IgG2a κ isotype controls from BD Pharmingen (BD Biosciences,
275 Franklin Lakes, NJ, USA). Flow cytometry analysis was performed using a FACS Canto II flow cytometer
276 and FlowJo (v10) software (BD Biosciences, Franklin Lakes, NJ, USA). Delta mean fluorescence intensity
277 (ΔMFI) was calculated by subtracting the mean MFI count in the SDC group from single MFI counts in
278 the four study groups. The Wilcoxon–Mann–Whitney test was used to test statistical differences
279 within the four study groups.

280 Validation cohorts

281 *Validation studies* were conducted using whole blood bulk RNA-seq data from two prospective,
282 multicenter European and Latin America cohorts, PREDICT and ACLARA (7,38). The inclusion and
283 exclusion criteria of both cohorts are shown in **Supplementary Tables 7 and 8**. Both cohorts collected
284 various measures, including clinical, pharmacological, and outcome data from AD patients upon
285 hospital admission and during follow-up visits (**Supplementary Tables 9 and 10**). The follow-up period
286 was 90 days for PREDICT and 28 days for ACLARA (**Supplementary Figures 5 and 6**). 90 days after study
287 inclusion, AD patients from the *PREDICT* cohort were categorized into SDC/UDC and pre-ACLF (7).
288 *ACLARA* patients were classified either into AD or pre-ACLF. The diagnostic criteria of ACLF in both
289 cohorts were according to the EF-CLIF definition (5).

290 The criteria for inclusion in our investigation were AD at hospital admission, availability of data on
291 short-term outcomes (liver transplant, ACLF development, or death), clinical data, treatment, and
292 availability of biological samples (buffy coat, tempus, serum, and plasma). Based on these criteria, 768
293 AD patients from PREDICT were chosen for analysis, with 738 samples passing quality control after
294 sequencing. According to the definition of ACLF within the discovery cohort, only patients who
295 developed ACLF within 28 days after hospital admission were included (n=61, **Supplementary Figure**
296 **7**). For the ACLARA cohort, the same criteria applied, with the added requirement that samples be
297 available at the Barcelona EFCLIF biobank by the end of March 2021 due to COVID-19-related delays
298 in shipping from South America. From ACLARA, 549 AD cirrhosis patients were selected, with 32
299 lacking buffy coat samples and 27 failing quality control after sequencing (**Supplementary Figure 8)**.
300 In total, 689 patients from PREDICT and 521 patients from ACLARA were included to validate the
301 single-cell results.

302 *PREDICT & ACLARA bulk RNA-seq*

303 Whole blood RNA-seq from 1,210 patients with AD included in the PREDICT (n=689) (7) and the
304 ACLARA (n=521)(38) studies were conducted according to the above-described bulk RNA-seq protocol.

305 A module score was calculated for each evaluated sample group, obtaining a gene signature score, as
306 described in Material and Methods: Module scores. Pearson (parametric) and Spearman (non-
307 parametric) correlation coefficients were computed to assess the relationships between the module
308 score and clinical variables. The Area Under the Receiver Operating Characteristic (AUC-ROC) curve
309 using the "*pROC"* R package (39) was utilized to evaluate the relationship between the module score
310 and outcomes (40). The comparison of ROC curves was performed using DeLong's Test. The analysis
311 of mean differences in the computed module scores among patient groups was assessed using the
312 ANOVA test when more than two groups were compared and the Wilcoxon Signed-Rank test
313 otherwise.
314

Statistical Methods

All analyses were performed in the R Computing Environment version 4.0.3 (41). Statistical methods are described in detail above in each subsection. In all statistical analyses, we considered *p*-value < 0.05 as statistically significant. In case an adjusted p-value for multiple testing is considered, it is described in the text.

321 ## Results

322 ### *Single-cell study cohort and sample description*

323 In total, 63 patients with AD and 15 healthy controls were prospectively recruited in 5 European
324 centers. After 90 days, patients were classified as having no readmission due to AD (SDC), readmission
325 due to AD (UDC), or ACLF development within the first 28 days (pre-ACLF). Of those, 16 patients (6
326 SDC, 6 UDC, 4 pre-ACLF) and four healthy controls were selected for single-cell analysis (see Material
327 and Methods; **Figure 1 A**). Respective PBMC samples subsequently underwent CITE-seq; bulk RNA-seq
328 on whole blood from the same patients was also performed (**Figure 1 B**). The median age at the time
329 of hospital admission was 60 years in the SDC, 57 years in the UDC, and 74 years in the pre-ACLF group
330 (**Table 1**). Of all patients, 75% were males, and 50% had been diagnosed with alcohol-related liver
331 cirrhosis. Previous episodes of acute decompensation were common in the UDC (4/6 patients) and
332 pre-ACLF (3/4 patients) groups. The primary reason for hospital admission in all groups was ascites.
333 Bacterial infection was present in 2 out of 6 SDC patients, and spontaneous bacterial peritonitis (SBP)
334 was evident in 2 out of 4 pre-ACLF patients. MELD and CLIF-C AD scores were significantly higher in
335 the pre-ACLF group compared to the SDC and the UDC groups (20 and 59 points, respectively).
336 Treatment at blood draw was not significantly different between the groups. All pre-ACLF patients
337 developed ACLF during their first hospital admission. Within the pre-ACLF group, one patient died, and
338 one patient underwent a liver transplant during follow-up. Additional baseline characteristics are
339 presented in **Supplementary Tables 3, 4, and 5**.

340 ### *An increase in circulating classical monocytes is associated with ACLF development*

341 For the single-cell transcriptional analysis, 130,846 cells, with a median of 1,632 genes per cell, were
342 recovered from the 20 individuals included in this study (**Figure 1 A**). We identified 11 cell clusters
343 corresponding to classical monocytes, non-classical monocytes, $CD4^+$ T cells, $CD8^+$ T cells, B cells, NK
344 cells, MAIT cells, dendritic cells, regulatory T cells, dnT cells, and gdT cells (**Figure 2 A, Supplementary**
345 **Figures 2**). Cell annotation was confirmed by cell surface marker profiling (**Supplementary Figure 3 A,**
346 **B**).

347 Aiming to identify changes in cellular proportions associated with disease progression, we compared
348 the cell composition among healthy controls, SDC, UDC, and pre-ACLF groups. We observed marked
349 proportion variations when investigating the most prevalent cell subtypes (those representing at least
350 1% of the total cells) (**Figure 2 B, C**). As expected, we found a significant increase of classic monocytes
351 in AD patients compared to healthy controls, with pre-ACLF exhibiting the highest fold change,
352 followed by UDC and SDC. Non-classical monocytes also increased significantly in the pre-ACLF
353 patients but to a lesser extent. Regarding T cell populations, $CD8^+$ T cells in AD patients decreased
354 compared to healthy controls. Similar trends were observed in cell proportions derived from surface
355 protein markers´ data (**Supplementary Figure 3 C, D**).

356 To examine the transcriptional changes within each cell population, we conducted a differential
357 expression analysis (DEA) across all groups of AD patients and healthy controls. We identified varying
358 numbers of differentially expressed genes (DEGs) in each cell type and contrast (SDC vs. healthy
359 controls, UDC vs. healthy controls, pre-ACLF vs. healthy controls) (**Figure 2 D**). Classical monocytes
360 showed the highest number of DEGs in both the total of all comparisons and each comparison

361 individually. In detail, pre-ACLF comparisons with SDC and UDC, respectively, showed that they
362 exhibited the highest number of DEGs, especially in classical monocytes (**Figure 2 E and**
363 **Supplementary Figure 9**).

364 Altogether, we identified perturbations in the peripheral immune cell landscape in AD patients
365 compared to healthy controls, with a notable accentuation of the monocytic population, especially in
366 the pre-ACLF patients.

367 ***Identification of classical monocyte subpopulations and their association with AD progression***

368 Given the observed alterations in both the cell proportion and gene expression of classical monocytes
369 in AD patients compared to healthy controls, we aimed to further explore the role of this cell
370 population in disease progression by identifying distinct classical monocytic subpopulations. To this
371 end, we applied unsupervised clustering to the classical monocytes, identifying three major cell
372 subclusters labelled as C0, C1, and C2 (**Figure 3 A**). C0 constituted the highest proportion of classical
373 monocytes, followed by C1 and C2.

374 Next, we aimed to investigate differences in the identified monocytic subclusters within the four
375 clinical groups. Similar to the overall monocyte population, an increase in the three monocyte
376 subpopulations was observed in AD patients compared to healthy controls (**Figure 3 B, Supplementary**
377 **Figure 10**). Specifically, C0 increased significantly in all AD groups, C1 was significantly enriched in UDC
378 and pre-ACLF patients, and C2 only in the pre-ACLF patients (**Figure 3 C**). Interestingly, within the pre-
379 ACLF group, the proportions of C1 and C2 monocytes increased according to the latency of ACLF onset
380 (**Figure 3 B)**. To further investigate the dynamic processes underlying the monocyte compartment,
381 trajectory analysis was complemented, which identified a continuous process from C0 to C2, with C1
382 representing a transitional state between C0 and C2 monocytes (**Figure 3 D**).

383 In the next step, we aimed to elucidate the functional and pathophysiological characteristics of the C2
384 subset. We first explored the transcriptional profile of monocytic markers with known biological
385 function in these cells (**Figure 3 E**). In contrast to the C0 subset, we observed lower expression of *CD14*,
386 as well as of genes encoding HLA-DR subunits (*HLA-DRA*) or isoforms (*HLA-DRB1*) in the C2 cluster.
387 Moreover, the expression of genes encoding pro-inflammatory mediators from the S100 protein
388 family, as well as antibacterial agents such as lysozyme (*LYZ*), were decreased within the C2 subset.
389 On the other hand, genes encoding proteins with regulatory functions in inflammatory and infection-
390 driven processes, such as *MERTK*, *VCAN*, *IRAK3*, *HIF1α*, and *TLR2*, showed increased expression
391 compared to C0. The expression of *CD15* was also higher in C2. C1 monocytes showed an intermediate
392 state between C0 and C2.

393 We then characterized transcriptional alterations by DEA of C2 subcluster vs. C0 and C1 subclusters.
394 The exploration of the top 100 up- and downregulated genes confirmed the intermediate state of C1
395 (**Figure 3 F, Supplementary Figure 10)**. Interestingly, the upregulated genes illustrated a rather
396 heterogeneous biological pattern. In contrast, among the most downregulated genes, we observed
397 several genes that encode different proteins/enzymes involved in processes relevant to energy
398 production and metabolism. These genes included ATP-production genes (i.e. gene: *ATP5F1E*/protein:
399 ATP synthase F1 subunit epsilon**;** *ATP5MG*/ATP synthase membrane subunit g) and oxidative
400 phosphorylation genes (*UQCR11*/ubiquinol-cytochrome c reductase, complex III sub-unit XI;

401 *COX7C*/cytochrome c oxidase subunit 7C; *COX8A*/cytochrome c oxidase subunit 8A). In total, three
402 genes that encode ATP synthase membrane subunits and six that encode cytochrome c oxidase
403 subunits were among the 50 most downregulated genes in the C2 subset compared to C0/C1.
404 Moreover, among the downregulated genes, we found numerous S100 proteins described as
405 important regulators of stress and inflammatory responses (**Supplementary Figure 10**).

406 Given the transcriptional profile of C2 classical monocytes, showing a decreased expression of the
407 surface receptor *HLA-DR*, we wondered whether this translates at the protein level. Hence, we
408 assessed the HLA-DR profile by flow cytometry on classical monocytes enriched from PBMCs from the
409 same AD and healthy control individuals**.** To analyze differences of the HLA-DR expression between
410 the groups, the delta of the mean fluorescence intensity (ΔMFI) of HLA-DR was calculated by
411 subtracting the mean MFI count in the SDC group from single MFI counts in the four study groups.
412 Even if the entire population of classical monocytes was considered in this approach, we still observed
413 a statistical tendency towards a decreased relative HLA-DR expression in patients with pre-ACLF
414 (**Figure 3 G**).

415 Thus, we identified a distinct monocytic whose abundance is associated with future ACLF
416 development. This subcluster is predominantly characterized by decreased expression of genes
417 involved in cellular energy supply.
418

419 ***Functional characterization of the classical monocyte subsets***

420 To further elucidate the biological functions of the monocyte subsets identified, we performed gene
421 set enrichment analysis (GSEA) comparing C2 and C0, with C1 considered an intermediate state. Our
422 analysis revealed a significant global downregulation of pathways related to energy metabolism,
423 including "*oxidative phosphorylation (OXPHOS)*" and "*aerobic respiration*" – both representing the
424 most overall regulated pathways in this data set–, as well as "*ATP biosynthetic process*" in the C2
425 subset (**Figure 4 A** and **Supplementary Table 11**). Additionally, we investigated how these biological
426 processes were regulated in the different subclusters (C0, C1, and C2) (**Figure 4 B**) and in the different
427 patient subgroups (healthy controls, SDC, UDC, and pre-ACLF) (**Figure 4 C**). Importantly, our findings
428 indicated that C2 had significantly lower signature scores than C0 and C1 subclusters independently
429 of the clinical course.

430 Since bacterial infection represents a complication of cirrhosis-associated immune dysfunction and a
431 critical driver of ACLF progression, we also examined pathways related to the immune response in the
432 C2 monocytes (**Figure 4 D**). Although no significantly regulated pathways were identified based on
433 adjusted p-value, we observed a tendency towards a reduced activity of pathways related to the
434 immune response in C2 monocytes. Among them, we identified "*positive regulation of inflammatory*
435 *response*", "*defense response to bacterium*", and "*cytokine production*" (**Figure 4 D** and
436 **Supplementary Table 11**).

437 Hence, C2 monocytes exhibit an extensive impairment of pathways related to cellular energy supply
438 and a tendency towards a dysfunctional immune response.

439 ***Identification and translation of a C2 monocytic gene signature to whole blood profiles***

440 Given the identification of a specific population of C2 monocytes expanded in pre-ACLF patients by
441 CITE-seq of the PBMCs and the availability of transcriptional data from the whole blood of the same
442 patients (**Figure 1 B**), we aimed to investigate whether a C2-associated gene signature could still be
443 detected in whole blood in the included patients. First, based on scRNA-seq data, we selected genes
444 to define such a signature by combining three criteria: (i) they were upregulated in classical monocytes
445 when compared with the rest of the cell types; (ii) they were upregulated when comparing C2 with
446 the other subtypes of classical monocytes; and (iii) they were upregulated within C2 when comparing
447 pre-ACLF and healthy controls/SDC/UDC. As a result, we identified 96 upregulated genes that
448 characterize the C2 monocytes subset in pre-ACLF patients (**Figure 5 A**).

449 Next, we analyzed the expression profiles of these 96 genes at the whole blood level. 94 genes were
450 expressed at the bulk level. Then, we selected those genes with a fold change higher than 25% in bulk
451 RNA-seq, equivalent to log2 FC> 0.32, for the three comparisons: healthy controls/SDC/UDC vs. pre-
452 ACLF. As a result, we identified 18 genes defining the C2-signature at whole blood level: *SLC11A1*,
453 *NAMPT*, *SMAP2*, *CD55*, *ACSL1*, *NEAT1*, *DLEU2*, *IRAK3*, *KYNU*, *TBXAS1*, *FKBP5*, *NUMB*, *PHF21A*, *AOAH*,
454 *ZFAND3*, *LYN*, *SLCO3A1*, and *PTEN* (**Figure 5 B**).

455 Subsequently, we computed an activity score associated with the defined C2 signature to assess its
456 profile in both single-cell PBMC and whole-blood RNA-seq data (**Figure 5 C, D**). We computed such
457 activity value using a signature score (see Material and Methods: Module scores), in which higher
458 values indicate high activity of the gene sets in a given sample or cell. As expected, we observed a
459 significant progressive increase in the C2 signature activity score from healthy controls to SDC and
460 UDC, culminating in the pre-ACLF group, which showed the highest levels at both the single-cell
461 (PBMCs) (**Figure 5 C**) and bulk (whole blood) levels (**Figure 5 D**).

462 These findings highlight the efficient translation of the C2 monocytic signature from the cellular to the
463 systemic level and its enrichment in pre-ACLF patients.

464 ***Validation of C2 gene signature in two prospective multicenter cohorts of patients with AD***

465 To validate the clinical significance of the defined C2 gene signature, we evaluated its relevance in two
466 large and independent prospective multicenter cohorts of patients with AD from Europe (PREDICT;
467 n=689) and from Latin America (ACLARA; n=521) (**Figure 6 A**). In both cohorts, whole blood samples
468 were collected at hospital admission, and bulk RNA-seq was performed. In PREDICT, patients were
469 followed up for 90 days and classified as SDC, UDC or pre-ACLF based on their clinical trajectory
470 (**Supplementary Figure 4, Supplementary Table 9**). In the ACLARA cohort, patients were followed up
471 for 28 days and classified as either AD or pre-ACLF (**Supplementary Figure 5, Supplementary Table**
472 **10)**. Detailed description of patient selection from both cohorts are provided in the Material and
473 Methods section and **Supplementary Figures 6 and 7**.

474 After computing the C2 signature activity score in both the PREDICT and ACLARA cohorts, we observed
475 a significant positive correlation with indicators of liver disease severity, including total bilirubin,
476 MELD, and CLIF-C AD score in patients from both cohorts at hospital admission (**Figure 6 B and**
477 **Supplementary Tables 12, 13**). In line, it was significantly enriched in the pre-ACLF group as well as in

478 non-survivors in both cohorts (**Figure 6 C, D**), emphasizing the identified classical monocyte subtype
479 (C2) to be associated with disease severity, AD progression, and fatal outcome in patients with AD.

480 In the next step, we asked which pathophysiological processes might primarily be associated with an
481 increased expression of the C2 gene signature in patients with AD. We performed additional
482 correlation analysis between the C2 gene signature score and clinical and laboratory parameters of
483 AD patients from both cohorts at hospital admission. We found a significant positive correlation of the
484 C2 score with white blood cell count and C-reactive protein in both cohorts (**Supplementary Figure 11**
485 **A and Supplementary Tables 12, 13**). Moreover, upon dividing the cohorts into patients with and
486 without bacterial infection, we observed additionally higher C2 signature activity scores in patients
487 with bacterial infection compared to those without infection in patients from the SDC and UDC groups
488 of the PREDICT cohort (**Supplementary Figure 11 B**).

489 The C2 signature activity score had an AUROC for ACLF or death in both PREDICT and ACLARA cohorts
490 around 0.65 (**Figure 6 E)**. However, combining the newly identified C2 signature score with the CLIF-C
491 AD score did not significantly improve the latter´s predictive capability regarding outcomes of ACLF
492 and death (**Supplementary Figure 12**).

493 In summary, we demonstrated that the C2 signature can be detected in whole blood RNA-seq data
494 from patients with AD and, most importantly, is associated with the progression to ACLF and mortality
495 in two independent cohorts. Additionally, we showed that the C2 signature provides predictive value
496 beyond the presence of bacterial infection.

497 ## Discussion

498 In this European multicenter study, we prospectively investigated the transcriptomic alterations of
499 peripheral immune cells at single-cell resolution in patients with AD. We found that classical
500 monocytes showed the most pronounced transcriptional regulation among the investigated immune
501 cells. A monocytic subpopulation, termed C2, was identified that correlated with the onset of ACLF.
502 This subpopulation was characterized by impaired cellular energy supply. Notably, the transcriptomic
503 signature of these cells remained significantly associated with bacterial infection, ACLF development,
504 and mortality in whole-blood bulk RNA-seq data of two large prospective multicenter cohorts of
505 patients with AD.

506 While previous studies represent case-control studies focusing on ACLF (18–20), our study is the first
507 to prospectively analyze changes in peripheral immune cells in patients with AD *before* ACLF
508 development. Classical monocytes were identified to show the highest transcriptional regulation of all
509 investigated immune cells during AD. Various studies have consistently reported an
510 overrepresentation of monocytic gene signatures among regulated genes in the blood of patients with
511 manifest ACLF (17,18). Our analysis revealed that those significant transcriptional alterations
512 identified in classical monocytes, in fact, can be observed much earlier in the course of the disease,
513 even in the early stages of AD. These findings indicate monocytes to play a pivotal role in AD and
514 support their involvement in disease progression.

515 In-depth exploration of classical monocytes identified three major subclusters: C0, C1, and C2. The C2
516 subcluster showed an expanded presence in pre-ACLF patients (up to 10%) and correlated with latency
517 towards ACLF. C1 appeared as an intermediate state, illustrating the progressive alterations in
518 monocyte populations as cirrhosis advances. Consequently, we focused our analysis on the differences
519 between the C0 and C2 subclusters. Interestingly, the C2 subset was not only detectable in patients
520 with pre-ACLF but – to a lesser extent – already in healthy controls and patients from the other AD
521 groups. This suggests that the C2 monocytic subpopulation already exists in physiological conditions
522 and expands as the disease progresses.

523 In 2018, Bernsmeier et al. described an expansion of mononuclear myeloid-derived suppressor cells
524 (M-MDSCs, $CD14^{+}HLADR^{lo/-}CD15^{-}$) in ACLF patients associated with impaired antimicrobial response
525 (42). We questioned whether our newly identified C2 subcluster shares features with M-MDSCs. While
526 the expression of *CD14, HLA-DR, CD163, CX3CR1,* and *CCR5* was decreased and pointed in the same
527 direction, the expression of *CD15, MERTK*, and *CD86* was increased, in contrast to the M-MDSC
528 phenotype. Furthermore, the expression of *S100A8* and *S100A9*, which encode for two pro-
529 inflammatory mediators preferentially secreted by M-MDSCs (42), were downregulated in the C2
530 subset. Thus, we propose that the C2 monocyte subpopulation represents a previously undescribed
531 monocyte subset associated with AD progression.

532 Additional transcriptomic profiling was conducted to further characterize the C2 subpopulation using
533 marker genes of monocyte differentiation and expansion during cirrhosis progression. Various genes
534 encoding proteins related to inflammatory and immune responses, including interleukin-1 receptor-
535 associated kinase 3 (*IRAK3*), hypoxia-inducible factor 1α (*HIF-1α*), and toll-like receptor 2 (*TLR2*), were
536 upregulated in the C2 subset. In contrast, we observed several genes encoding proteins associated
537 with *suppressed* immune responses to be increasingly expressed in C2 monocytes. For example,

538 *MERTK*, a tyrosine kinase receptor observed to be increasingly expressed on immunoregulatory
539 monocytes in patients with ACLF, was upregulated in the C2 subset (43). Further upregulated genes
540 included *VCAN*, which encodes versican and was found to be associated with an immunosuppressive
541 phenotype of monocytes in sepsis (44). On the other hand, distinct genes encoding pro-inflammatory
542 S100 proteins, including *S100A8, S100A9,* and *S100A12*, were downregulated in the C2 subset. Finally,
543 genes relevant to bacterial immune response, such as *CD68*, which is relevant for monocyte adhesion,
544 as well as *LYZ*, encoding for anti-bacterial lysozymes, were decreasingly expressed. In summary, the
545 C2 monocyte subcluster identified in this study is characterized by a distinct transcriptional profile
546 that partially reflects enhanced expression of genes related to immune stimulation. However, genes
547 associated with immunosuppression and, especially, impaired bacterial response were likewise
548 regulated. We hypothesized that the C2 subset reflects evidence of early immunological dysfunction
549 that might favor severe bacterial infections as pivotal precipitators of ACLF. Our hypothesis was
550 validated in whole blood bulk RNA-seq data from two large and independent cohorts, including more
551 than 1200 AD patients (PREDICT and ACLARA). Here, the C2 signature not only positively correlated
552 with liver disease severity but was significantly enriched in the pre-ACLF groups of both cohorts. But,
553 in accordance with our hypothesis that metabolic disturbances within the C2 monocytes favour
554 bacterial infection, the C2 signature was even more evident in AD patients with simultaneous bacterial
555 infections. These findings highlight the importance of the C2 signature not only in cirrhosis progression
556 but also in precipitating events that lead to ACLF.

557 To explore our findings in more detail, we conducted a pathway analysis uncovering the biological
558 functions of the newly identified C2 monocyte subset. While our analysis showed a clear trend of
559 reduced immune function within the C2 subset, immune-related pathways were not the most
560 significantly regulated. Instead, our analysis revealed a dominant downregulation of genes that
561 encode key enzymes in cellular energy supply. This aligns with reports from several studies, which
562 describe a progressive worsening of metabolic disturbances in patients with compensated cirrhosis,
563 AD, and ACLF, likely driven by systemic inflammation (19,45–48). We here identified the specific
564 monocytic subset that predominantly is characterized by bioenergetic failure and early signs of
565 immune exhaustion, reflecting the inflammation-associated immunometabolic changes associated
566 with cirrhosis progression (49,50).

567 Our findings are of translational relevance as they underline the hypothesis of systemic inflammation-
568 associated energetic exhaustion in patients before ACLF development. Systemic inflammation in
569 patients with cirrhosis is, in part, assumed to be driven by bacterial translocation. Hence, current
570 approaches targeting gut barrier function and intestinal microbiota diversity, such as rifaximin or fecal
571 microbiota transfer, are investigated to prevent AD or ACLF development in patients with chronic liver
572 disease (51,52). The fact that we identified a monocytic subset that is characterized by bioenergetic
573 failure and expands before ACLF development further supports therapeutic strategies that aim to
574 prevent inflammation-induced bioenergetic failure in patients with AD. Moreover, the identified
575 monocytic subset could serve as a cellular model to develop and test such therapeutic strategies that
576 aim to reduce systemic inflammation-induced immune cell exhaustion.

577 Despite the valuable insights gained from this study, complementary omics or functional assays are
578 needed to mechanistically validate our findings and pinpoint potential intervention targets. Moreover,

579 longitudinal single-cell analyses would be beneficial to help understand the dynamic changes in
580 monocyte subsets over the disease course.

581 In summary, our analysis presents strong evidence supporting the involvement of monocytes,
582 particularly a novel subset referred to as C2, in cirrhosis progression and ACLF development. We offer
583 valuable insights into transcriptional alterations in these cells, highlighting a state of immuno-
584 metabolic exhaustion that may increase susceptibility to bacterial infections. Our findings support the
585 idea that preventing the bioenergetic failure of immune cells during cirrhosis progression represents
586 a promising therapeutic target.
587

Acknowledgements: We thank all participating centres for their efforts in patient recruitment and fruitful collaboration. We thank the Genomics Facility of the Interdisciplinary Center for Clinical Research (IZKF) Aachen for sequencing experiments. Special thanks go to Jasmin Hübner and Anna Rudzinski for their extraordinary help in sequencing the samples.

Conflicts of interest: Jonel Trebicka has received speaking and/or consulting fees from Astra-Zeneca, Gore, Boehringer-Ingelheim, Falk, Grifols, Genfit, and CSL Behring. T Bruns received consulting fees from Intercept/Advanz Pharma, Grifols, Sobi, and SmartDyeLivery. Paolo Caraceni has received speaking and/or consulting fees from Grifols SA , Octapharma SA, CSL Behring, and Gilead.

Data availability statement: Researchers who provide a methodology sound proposal can apply for the data, as far as the proposal is in line with the research consented by the patients. These proposals should be requested through https://www.clifresearch.com/decision/Home.aspx. Data requestors will need to sign a data transfer agreement. Single-cell data is currently being uploaded to the European Genome-phenome Archive (EGA).

Ethics approval statement: The studies involving human participants were reviewed and approved by the Ethical Board of all five participating centres in Europe. The patients/participants provided written informed consent to participate in this study.

Funding:
This project has received funding from the European Union's Horizon 2020 research and innovation program under grant agreement No 847949. This research was made possible through access to data generated by the PREDICT and ACLARA studies promoted and funded by the European Foundation for the Study of Chronic Liver Failure (EF-CLIF), a private, non-profit organization supported by unrestricted grants from Grifols and Genfit.

T.H.W. received financing from the START program of the RWTH Aachen University.

N.P.P. was funded by a Ramón y Cajal fellow (RYC2021-032197-I) from the MCIN/AEI/10.13039/501100011033 and European Union "NextGenerationEU"/PRTR and by a Juan de la Cierva-formación fellow (FJC2019-042304-I) from the Spanish Ministry of Science and Innovation (MCIN).

T.B. was supported by the German Research Foundation (SFB1383 Project ID 403224013/B07).

The Genome Analysis Platform in CIC bioGUNE is supported by the Basque Department of Industry, Tourism and Trade (Etortek, Elkartek and Emaitek Programs), the Innovation Technology Department of Bizkaia County, CIBERehd Network, and Spanish MINECO the Severo Ochoa Excellence Accreditation (CEX2021-001136-S).

JC laboratory is supported by Ministerio de Ciencia e Innovación/Agencia Estatal Investigación MCIN/AEI (PID2022-138970OB-I00 10.13039/501100011033/FEDER, UE). C.T. was supported by the DFG grants TR285/10-2 and SFB CRC1382, A08 (ID 403224013).

PER research laboratory is supported by the Fondation pour la Recherche Médicale (FRM EQU202303016287), "Institut National de la Santé et de la Recherche Médicale" (ATIP AVENIR), the "Agence Nationale pour la Recherche" (ANR-18-CE14-0006-01, RHU QUID-NASH, ANR-18-IDEX-0001,

ANR-22-CE14-0002) by « Émergence, Ville de Paris », by Fondation ARC and by France 2030 RHU LIVER-TRACK (ANR-23-RHUS-0014).

D.G.-C. research laboratory is supported by King Abdullah University of Science and Technology.

Authors´ contributions: THW, RK, JC, PER, CT, and DGC designed the study. THW, MRP, MB, GZ, DB, MS, WG, RS, SV, AV, DC, and IG supervised patient recruitment and sample collection and assessed clinical data. THW, MRP, FS, AMA and JR performed experiments. SPE led and performed data assessment, analysis, and visualization. THW, DGC, NP, CLV and EH supported data assessment, analysis, and visualization. THW, SPE, MRP, DGC, NP, and EH performed data interpretation. THW, SPE, NP, and DGC wrote the manuscript. EH, MRP, FS, JR, AK, RK, TB, PC, CA, NK, JT, JC, PER, and CT revised the manuscript. All authors provided intellectual input and approved the final version of the manuscript.

640 ## References

641 1. Ginès P, Krag A, Abraldes JG, Solà E, Fabrellas N, Kamath PS. Liver cirrhosis. The Lancet. 2021
642 Oct;398(10308):1359–76.
643 2. Mansour D, McPherson S. Management of decompensated cirrhosis. Clin Med (Lond). 2018
644 Apr 1;18(Suppl 2):s60–5.
645 3. Engelmann C, Clària J, Szabo G, Bosch J, Bernardi M. Pathophysiology of decompensated
646 cirrhosis: Portal hypertension, circulatory dysfunction, inflammation, metabolism and
647 mitochondrial dysfunction. Vol. 75, Journal of Hepatology. Elsevier B.V.; 2021. p. S49–66.
648 4. D'Amico G, Morabito A, D'Amico M, Pasta L, Malizia G, Rebora P, et al. Clinical states of cirrhosis
649 and competing risks. J Hepatol. 2018 Mar;68(3):563–76.
650 5. Moreau R, Jalan R, Gines P, Pavesi M, Angeli P, Cordoba J, et al. Acute-on-chronic liver failure
651 is a distinct syndrome that develops in patients with acute decompensation of cirrhosis.
652 Gastroenterology. 2013 Jun;144(7):1426–37, 1437.e1-9.
653 6. Gustot T, Stadlbauer V, Laleman W, Alessandria C, Thursz M. Transition to decompensation and
654 acute-on-chronic liver failure: Role of predisposing factors and precipitating events. J Hepatol.
655 2021 Jul;75 Suppl 1:S36–48.
656 7. Trebicka J, Fernandez J, Papp M, Caraceni P, Laleman W, Gambino C, et al. The PREDICT study
657 uncovers three clinical courses of acutely decompensated cirrhosis that have distinct
658 pathophysiology. J Hepatol. 2020 Oct 1;73(4):842–54.
659 8. Albillos A, Martin-Mateos R, Van der Merwe S, Wiest R, Jalan R, Álvarez-Mon M. Cirrhosis-
660 associated immune dysfunction. Nat Rev Gastroenterol Hepatol. 2022 Feb;19(2):112–34.
661 9. Arroyo V, Angeli P, Moreau R, Jalan R, Clària J, Trebicka J, et al. The systemic inflammation
662 hypothesis: Towards a new paradigm of acute decompensation and multiorgan failure in
663 cirrhosis. J Hepatol. 2021 Mar;74(3):670–85.
664 10. Clària J, Arroyo V, Moreau R. Roles of systemic inflammatory and metabolic responses in the
665 pathophysiology of acute-on-chronic liver failure. JHEP Reports. 2023 Sep;5(9):100807.
666 11. Clària J, Stauber RE, Coenraad MJ, Moreau R, Jalan R, Pavesi M, et al. Systemic inflammation in
667 decompensated cirrhosis: Characterization and role in acute-on-chronic liver failure.
668 Hepatology. 2016 Oct;64(4):1249–64.
669 12. Engelmann C, Sheikh M, Sharma S, Kondo T, Loeffler-Wirth H, Zheng YB, et al. Toll-like receptor
670 4 is a therapeutic target for prevention and treatment of liver failure. J Hepatol. 2020
671 Jul;73(1):102–12.
672 13. Clària J, Arroyo V, Moreau R. The Acute-on-Chronic Liver Failure Syndrome, or When the Innate
673 Immune System Goes Astray. J Immunol. 2016 Nov 15;197(10):3755–61.
674 14. Trebicka J, Bork P, Krag A, Arumugam M. Utilizing the gut microbiome in decompensated
675 cirrhosis and acute-on-chronic liver failure. Nat Rev Gastroenterol Hepatol. 2021
676 Mar;18(3):167–80.
677 15. Wasmuth HE, Kunz D, Yagmur E, Timmer-Stranghöner A, Vidacek D, Siewert E, et al. Patients
678 with acute on chronic liver failure display "sepsis-like" immune paralysis. J Hepatol. 2005
679 Feb;42(2):195–201.
680 16. Martin-Mateos R, Alvarez-Mon M, Albillos A. Dysfunctional Immune Response in Acute-on-
681 Chronic Liver Failure: It Takes Two to Tango. Front Immunol. 2019;10:973.
682 17. Weiss E, de la Grange P, Defaye M, Lozano JJ, Aguilar F, Hegde P, et al. Characterization of Blood
683 Immune Cells in Patients With Decompensated Cirrhosis Including ACLF. Front Immunol. 2021
684 Feb 5;11.
685 18. Yao J, Liu T, Zhao Q, Ji Y, Bai J, Wang H, et al. Genetic landscape and immune mechanism of
686 monocytes associated with the progression of acute-on-chronic liver failure. Hepatol Int. 2023
687 Jun 10;17(3):676–88.

688 19. Feio-Azevedo R, Boesch M, Radenkovic S, van Melkebeke L, Smets L, Wallays M, et al. Distinct
689 immunometabolic signatures in circulating immune cells define disease outcome in acute-on-
690 chronic liver failure. Hepatology. 2024 May 16;
691 20. Yao J, Ji Y, Liu T, Bai J, Wang H, Yao R, et al. Single-Cell RNA Sequencing Shows T-Cell Exhaustion
692 Landscape in the Peripheral Blood of Patients with Hepatitis B Virus-Associated Acute-on-
693 Chronic Liver Failure. Gut Liver. 2024 May 15;18(3):520–30.
694 21. Zhang P, Li H, Zhou C, Liu K, Peng B, She X, et al. Single-Cell RNA Transcriptomics Reveals the
695 State of Hepatic Lymphatic Endothelial Cells in Hepatitis B Virus-Related Acute-on-Chronic Liver
696 Failure. J Clin Med. 2022 May 20;11(10):2910.
697 22. Ruitenberg JJ, Mulder CB, Maino VC, Landay AL, Ghanekar SA. VACUTAINER CPT and Ficoll
698 density gradient separation perform equivalently in maintaining the quality and function of
699 PBMC from HIV seropositive blood samples. BMC Immunol. 2006 May 25;7:11.
700 23. Zheng GXY, Terry JM, Belgrader P, Ryvkin P, Bent ZW, Wilson R, et al. Massively parallel digital
701 transcriptional profiling of single cells. Nat Commun. 2017 Jan 16;8(1):14049.
702 24. Dobin A, Davis CA, Schlesinger F, Drenkow J, Zaleski C, Jha S, et al. STAR: ultrafast universal
703 RNA-seq aligner. Bioinformatics. 2013 Jan 1;29(1):15–21.
704 25. Hao Y, Hao S, Andersen-Nissen E, Mauck WM, Zheng S, Butler A, et al. Integrated analysis of
705 multimodal single-cell data. Cell. 2021 Jun;184(13):3573-3587.e29.
706 26. Hafemeister C, Satija R. Normalization and variance stabilization of single-cell RNA-seq data
707 using regularized negative binomial regression. Genome Biol. 2019 Dec 23;20(1):296.
708 27. Butler A, Hoffman P, Smibert P, Papalexi E, Satija R. Integrating single-cell transcriptomic data
709 across different conditions, technologies, and species. Nat Biotechnol. 2018 May 2;36(5):411–
710 20.
711 28. Korsunsky I, Millard N, Fan J, Slowikowski K, Zhang F, Wei K, et al. Fast, sensitive and accurate
712 integration of single-cell data with Harmony. Nat Methods. 2019 Dec 18;16(12):1289–96.
713 29. Mulè MP, Martins AJ, Tsang JS. Normalizing and denoising protein expression data from
714 droplet-based single cell profiling. Nat Commun. 2022 Apr 19;13(1):2099.
715 30. Miller SA, Policastro RA, Sriramkumar S, Lai T, Huntington TD, Ladaika CA, et al. LSD1 and
716 Aberrant DNA Methylation Mediate Persistence of Enteroendocrine Progenitors That Support
717 *BRAF* -Mutant Colorectal Cancer. Cancer Res. 2021 Jul 15;81(14):3791–805.
718 31. Wu T, Hu E, Xu S, Chen M, Guo P, Dai Z, et al. clusterProfiler 4.0: A universal enrichment tool
719 for interpreting omics data. The Innovation. 2021 Aug;2(3):100141.
720 32. Qiu X, Mao Q, Tang Y, Wang L, Chawla R, Pliner HA, et al. Reversed graph embedding resolves
721 complex single-cell trajectories. Nat Methods. 2017 Oct 21;14(10):979–82.
722 33. Andrews S. http://www.bioinformatics.babraham.ac.uk/projects/fastqc. 2010. FastQC: a
723 quality control tool for high throughput sequence data.
724 34. Bolger AM, Lohse M, Usadel B. Trimmomatic: a flexible trimmer for Illumina sequence data.
725 Bioinformatics. 2014 Aug 1;30(15):2114–20.
726 35. Anders S, Pyl PT, Huber W. HTSeq—a Python framework to work with high-throughput
727 sequencing data. Bioinformatics. 2015 Jan 15;31(2):166–9.
728 36. Law CW, Chen Y, Shi W, Smyth GK. voom: precision weights unlock linear model analysis tools
729 for RNA-seq read counts. Genome Biol. 2014;15(2):R29.
730 37. Hänzelmann S, Castelo R, Guinney J. GSVA: gene set variation analysis for microarray and RNA-
731 Seq data. BMC Bioinformatics. 2013 Dec 16;14(1):7.
732 38. Farias AQ, Curto Vilalta A, Momoyo Zitelli P, Pereira G, Goncalves LL, Torre A, et al. Genetic
733 Ancestry, Race, and Severity of Acutely Decompensated Cirrhosis in Latin America.
734 Gastroenterology. 2023 Sep;165(3):696–716.
735 39. Robin X, Turck N, Hainard A, Tiberti N, Lisacek F, Sanchez JC, et al. pROC: an open-source
736 package for R and S+ to analyze and compare ROC curves. BMC Bioinformatics. 2011 Dec
737 17;12(1):77.

40. Hajian-Tilaki K. Receiver Operating Characteristic (ROC) Curve Analysis for Medical Diagnostic Test Evaluation. Caspian J Intern Med. 2013;4(2):627–35.
41. R Core Team. R: A language and environment for statistical computing. Vienna, Austria: R Foundation for Statistical Computing; 2021.
42. Bernsmeier C, Triantafyllou E, Brenig R, Lebosse FJ, Singanayagam A, Patel VC, et al. CD14+ CD15- HLA-DR- myeloid-derived suppressor cells impair antimicrobial responses in patients with acute-on-chronic liver failure. Gut. 2018 Jun;67(6):1155–67.
43. Bernsmeier C, Pop OT, Singanayagam A, Triantafyllou E, Patel VC, Weston CJ, et al. Patients with acute-on-chronic liver failure have increased numbers of regulatory immune cells expressing the receptor tyrosine kinase MERTK. Gastroenterology. 2015 Mar;148(3):603-615.e14.
44. Yao RQ, Zhao PY, Li ZX, Liu YY, Zheng LY, Duan Y, et al. Single-cell transcriptome profiling of sepsis identifies HLA-DRlowS100Ahigh monocytes with immunosuppressive function. Mil Med Res. 2023 Jun 19;10(1):27.
45. Li J, Liang X, Jiang J, Yang L, Xin J, Shi D, et al. PBMC transcriptomics identifies immune-metabolism disorder during the development of HBV-ACLF. Gut. 2022 Jan;71(1):163–75.
46. Maheshwari D, Kumar D, Jagdish RK, Nautiyal N, Hidam A, Kumari R, et al. Bioenergetic Failure Drives Functional Exhaustion of Monocytes in Acute-on-Chronic Liver Failure. Front Immunol. 2022 Jun 3;13.
47. Langer MM, Eickelmann C, Kleinbongard P, Lange CM. Impaired mitochondrial complex IV respiration in peripheral blood mononuclear cells discriminates acute-on-chronic liver failure from acute decompensation. J Hepatol. 2022 Sep;77(3):874–6.
48. Zhang IW, Curto A, López-Vicario C, Casulleras M, Duran-Güell M, Flores-Costa R, et al. Mitochondrial dysfunction governs immunometabolism in leukocytes of patients with acute-on-chronic liver failure. J Hepatol. 2022 Jan;76(1):93–106.
49. Wasmuth HE, Kunz D, Yagmur E, Timmer-Stranghöner A, Vidacek D, Siewert E, et al. Patients with acute on chronic liver failure display “sepsis-like” immune paralysis. J Hepatol. 2005 Feb;42(2):195–201.
50. Bernsmeier C, van der Merwe S, Périanin A. Innate immune cells in cirrhosis. J Hepatol. 2020 Jul;73(1):186–201.
51. Bajaj JS, Salzman NH, Acharya C, Sterling RK, White MB, Gavis EA, et al. Fecal Microbial Transplant Capsules Are Safe in Hepatic Encephalopathy: A Phase 1, Randomized, Placebo-Controlled Trial. Hepatology. 2019 Nov;70(5):1690–703.
52. Trebicka J, Macnaughtan J, Schnabl B, Shawcross DL, Bajaj JS. The microbiota in cirrhosis and its role in hepatic decompensation. J Hepatol. 2021 Jul;75 Suppl 1(Suppl 1):S67–81.

Figures

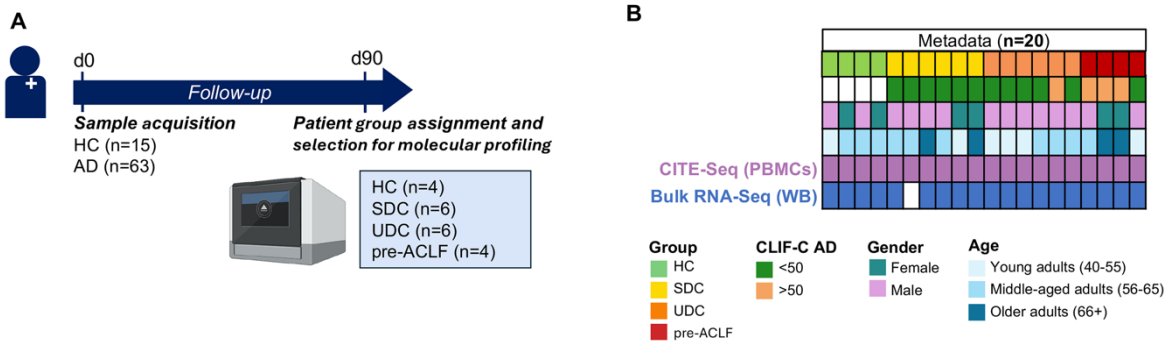

Figure 1. Study design.

(A) Schematic diagram of the study design. PBMC samples from 63 patients admitted with AD and 15 HC were collected. After 90 days of follow-up (d90), AD patients were classified as SDC, UDC, or pre-ACLF due to their clinical course. Of those, 16 patients and 4 HC were selected for scRNA-seq analysis. **(B)** Representation of the multi-omics approach along with the associated clinical metadata, including study group, CLIF-C AD score, gender, and age. *Abbreviations:* AD, acute decompensation; HC, healthy controls; PBMCs, peripheral blood mononuclear cells; pre-ACLF, pre-acute-on-chronic liver failure; SDC, stable decompensated cirrhosis; UDC, unstable decompensated cirrhosis.

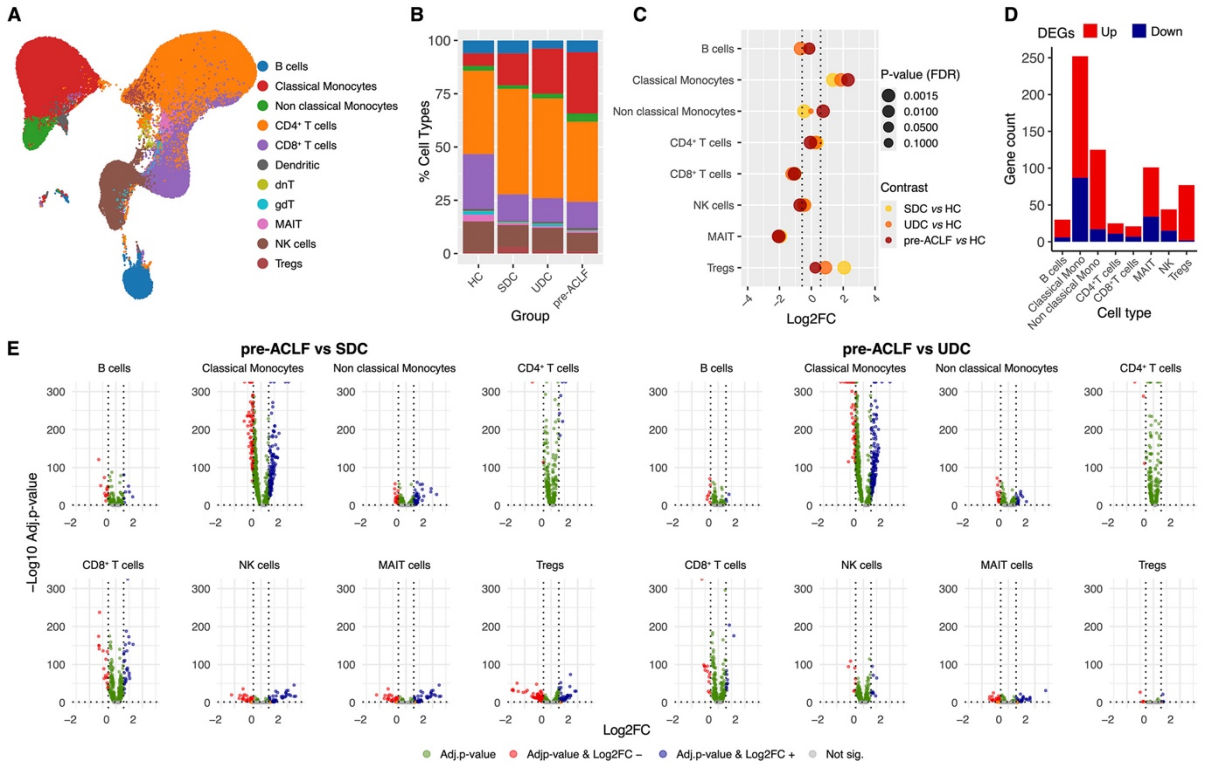

Figure 2. Single-cell transcriptional profiling of PBMCs from healthy controls and patients with SDC, UDC, and pre-ACLF.

(A) UMAP projection of the 143,952 PBMCs analyzed, colored by the 11 detected cell populations. **(B)** Barplot showing the variability of immune cell subsets between the different groups. **(C)** Cleveland plot showing the log2 fold-change for the eight main cellular subpopulations. For each cell type, pairwise comparisons were made: SDC *vs*. HC (yellow), UDC *vs.* HC (orange), and pre-ACLF *vs.* HC (dark red). Cell types were considered differentially expressed when the fold change (log2 FC; estimated using a bootstrapping confidence interval analysis) was > 0.58 (dashed vertical lines) and the adjusted p-value was < 0.05 (represented by the dot size; estimated using a permutation analysis). **(D)** Sum of the number of DEGs across cell types; a gene is considered significant if adjusted p-value < 0.05 (Benjamini-Hochberg) and absolute Fold Change > 1.5. **(E, F)** Volcano plots representing the fold change (log2 FC) and statistical significance (adjusted p-value) for different immune cell populations: B cells, classical monocytes, non-classical monocytes, CD4+ T cells, CD8+ T cells, NK cells, MAIT cells, and Tregs. The x-axis shows the log2 FC, while the y-axis represents the -log10 of the adjusted p-values for each gene. Points in red and blue indicate statistically significant changes (based on adjusted p-values) with positive or negative log2FC, respectively, while gray points indicate non-significant changes. **E,** illustrates the comparison of pre-ACLF against SDC, and **F,** illustrates the comparison of pre-ACLF against UDC. *Abbreviations:* AD, acute decompensation; HC, healthy controls; PBMC, peripheral blood mononuclear cells; pre-ACLF, pre-acute-on-chronic liver failure; NK cells, natural killer cells; MAIT cells, mucosal-associated invariant T cells; SDC, stable decompensated cirrhosis; Tregs, regulatory T cells; UDC, unstable decompensated cirrhosis.

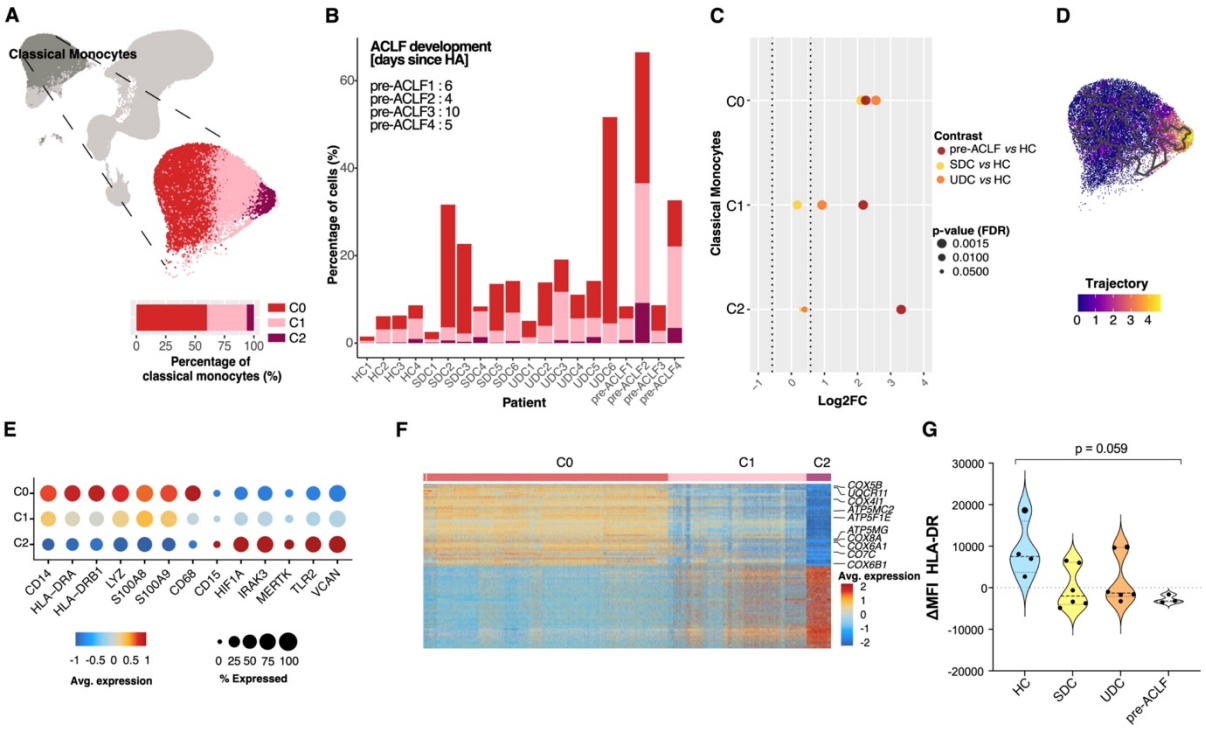

Figure 3. Identification of a classical monocyte subpopulation associated with ACLF development. **(A)** UMAP of all cell types with a zoom on classical monocytes with cells colored based on the subclusters C0, C1, and C2. **(B)** Relative percentages of each monocyte subcluster in each individual. **(C)** Cleveland plot showing the log2 fold-change in cell subtype prevalence for the 3 monocyte subclusters. For each subcluster, pairwise comparisons were made: SDC vs. HC, UDC vs. HC, and pre-ACLF vs. HC. Log2FC and FDR were estimated, respectively, using bootstrapping and permutation analysis. **(D)** UMAP with the pseudo-time trajectory on classical monocytes subclusters using Monocle3. **(E)** Dot plot indicating the expression of selected genes in each monocytic subcluster. **(F)** Heatmap displaying the scaled expression values of the top 50 up and downregulated genes in each subcluster. Please find extensive gene annotation in Supplementary Figure 10. **(G)** Violin plots illustrating the distribution, median, and IQR of the ΔMIF (subtraction of the mean MFI count in the SDC group from single MFI counts in the four study groups) of surface HLA-DR expression on classical monocytes. Samples were drawn from the single-cell study cohort, including healthy controls (n=4) and patients with SDC (n=6), UDC (n=6), and pre-ACLF (n=4). The Wilcoxon-Mann-Whitney test was used to test statistically significant differences in relative HLA-DR expression within the four study groups. *Abbreviations:* Avg, average; HC, healthy controls; Log2FC, logarithmic 2 Fold Change; pre-ACLF, pre-acute-on-chronic liver failure; SDC, stable decompensated cirrhosis; UDC, unstable decompensated cirrhosis; ΔMIF, delta of mean fluorescence intensity.

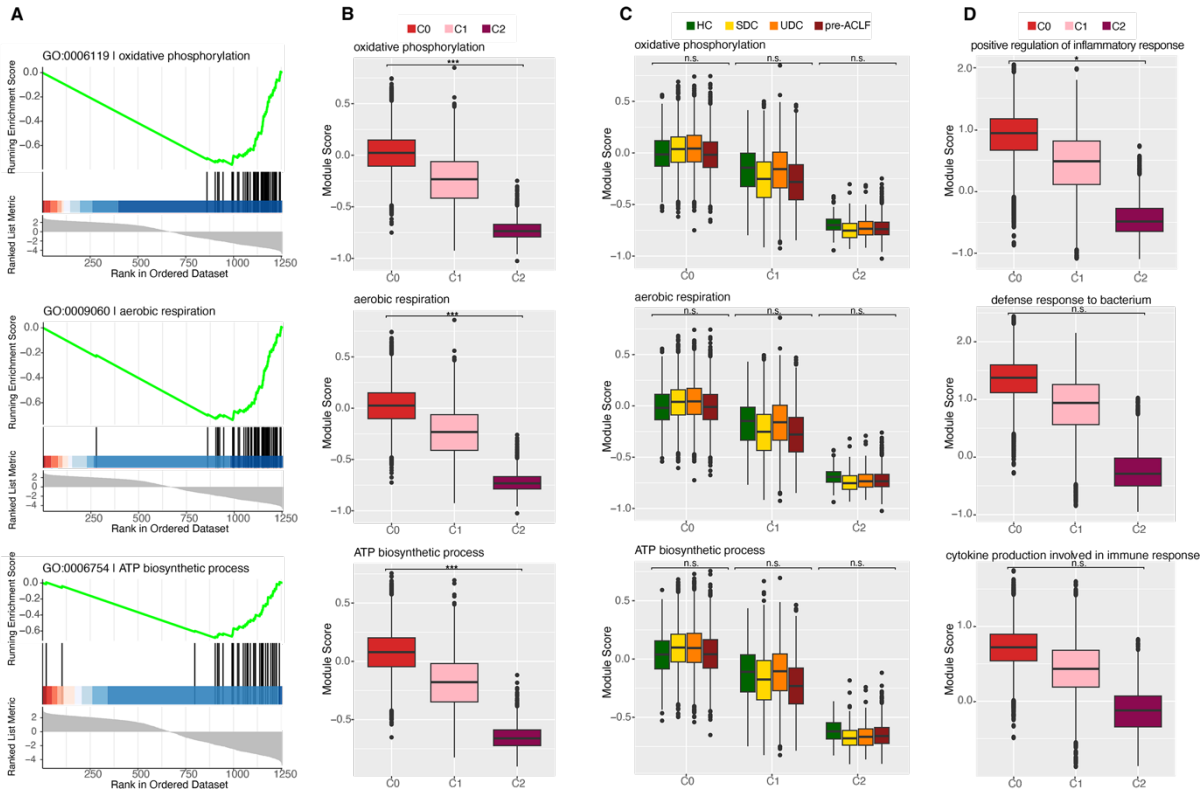

Figure 4. GSEA of key biological processes defining monocyte subpopulations.

(A) GSEA results for the three biological processes: oxidative phosphorylation, aerobic respiration, and ATP biosynthetic process. Running Enrichment Score (green line) depicts the cumulative enrichment score as genes are ranked by expression level. Ranked List Metric (bottom grey plot) shows the correlation of genes with the phenotype of interest across the ranked dataset. The heatmap (middle colored bar) represents the distribution of gene ranks—with red for positive correlation, blue for negative correlation, and white for a midpoint. **(B)** Boxplots showing the mean pathway signature score for the three processes for each monocyte subset and **(C)** for each group. Differences in module scores were assessed using Kruskal Wallis Test.***adjusted *p*-value <0.001; n.s. not significant**. (D)** Average gene expression trends across monocytic subsets related to Positive regulation of inflammatory response, Defense response to bacterium, and Cytokine production involved in immune response. Asterisks indicate reaching a significant nominal *p*-value, whereas the adjusted *p*-value was not significant. Differences in module scores were assessed using Kruskal Wallis Test. *nominal *p*-value <0.05. *Abbreviations:* n.s. not significant.

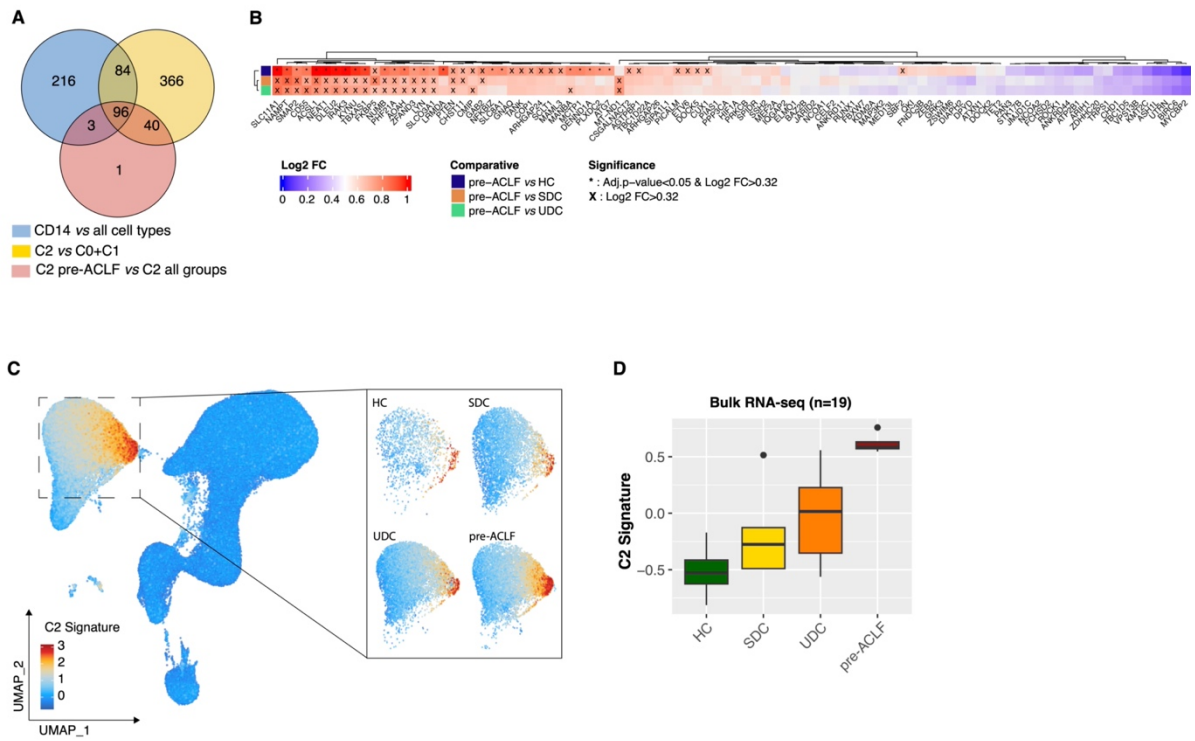

Figure 5. Identification of the C2 signature in whole blood RNA-seq data.
(A) Venn diagram illustrates the overlap of DEGs at single-cell resolution among three comparisons: classical monocytes versus all other cell types (blue), C2 versus Clusters 0 and 1 (yellow), and C2 pre-ACLF versus C2 in all groups (HC, SDC, and UDC (red). **(B)** Heatmap showing the scaled log2 FC levels of the selected DEGs from different comparatives in bulk RNA-seq: HC/SDC/ UDC vs. pre-ACLF. The color scale represents the log2 fold-change, with blue indicating downregulation and red indicating upregulation. Significant DEGs with log2 FC > 0.32 and adjusted p-value < 0.05 are marked with an asterisk; genes with a tendency (log2 FC > 0.32) are marked with a cross. **(C)** UMAP shows the distribution of the expression of the C2 signature. The inset panels show the distribution of C2 signature across different groups. **(D)** Boxplot displaying the module score for the C2 signature across the paired bulk RNA-seq data, categorized by group.

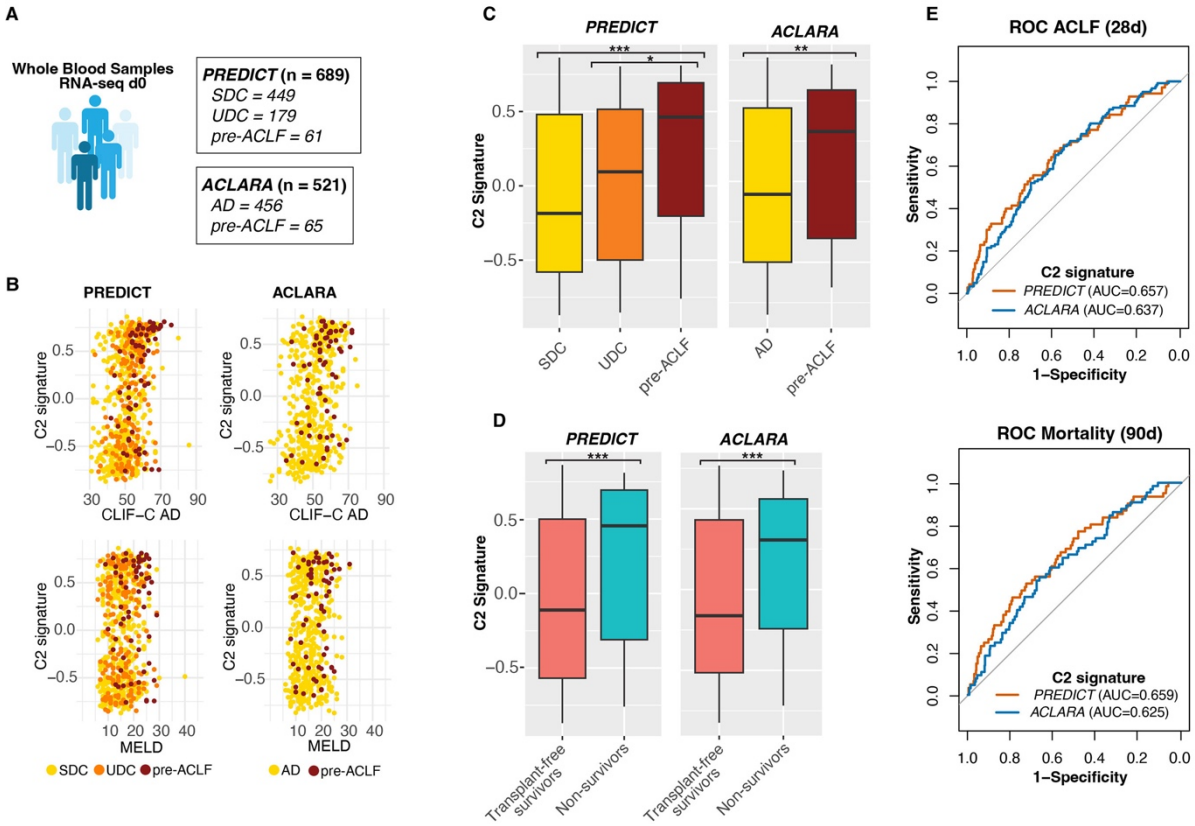

Figure 6. C2 monocytic subcluster validation in two independent AD cohorts.
(A) C2 signature was assessed in whole blood RNA-seq data collected at day 0 (d0) from two independent cohorts of AD patients. PREDICT cohort (top) accounted for data from 689 patients who were labeled 90 days after HA as SDC (n=449), UDC (n=179), or pre-ACLF (n=61). ACLARA (bottom) accounted for data from 521 patients who were labeled 28 days after HA as AD (n=456) or as pre-ACLF (n=65). **(B)** Correlation analysis of C2 signature values with CLIF-C AD and MELD across different patient groups in PREDICT (left) and ACLARA (right) cohorts. Top row: C2 signature vs. CLIF-C AD count. Bottom row: C2 signature vs. MELD levels. Each point represents an individual, colored by patient group: SDC, yellow; UDC, orange; pre-ACLF, dark red for the PREDICT cohort, and AD, yellow and pre-ACLF, dark red for the ACLARA cohort. **(C)** Boxplots display the average expression of the C2 signature among the different groups in PREDICT (left) and ACLARA (right) cohorts. Wilcoxon Signed-Rank Test was used to assess the differences between groups. **(D)** Boxplots display the average expression of the C2 signature between patients that died (pink) vs. patients that did not die (turquoise) in PREDICT (left) and ACLARA (right) cohorts Wilcoxon Signed-Rank Test was used to assess the differences between groups**. (E)** ROC curves showing the predictive capacity of the C2 signature regarding outcomes ACLF (top) and mortality (bottom) for the PREDICT (red) and the ACLARA (blue) cohorts. *** Adjusted *p*-value < 0.001; ** Adjusted *p*-value < 0.01; * Adjusted *p*-value < 0.05. *Abbreviations:* AD, acute decompensation; AUC, area under the curve; d0, day 0; HC, healthy controls; PBMC, peripheral blood mononuclear cells; pre-ACLF, pre-acute-on-chronic liver failure; ROC, Receiver-operating characteristic curve; SDC, stable decompensated cirrhosis; UDC, unstable decompensated cirrhosis.

879 **Table**

880

881 ***Table 1. Baseline characteristics of single-cell study cohort.***

	HC (n=4)	SDC (n=6)	UDC (n=6)	pre-ACLF (n=4)	*p*-value
Characteristics					
Age, median (range)	56 (52 - 64)	60 (54 - 81)	57 (51- 60)	74 (60 - 79)	0.063
Female Sex, yes, n (%)	2 (50)	2 (33)	0	2 (50)	0.248
Previous decompensations in the last 2 years, yes, n (%)	-	0	4 (67)	3 (75)	**0.023**
Cause of cirrhosis, n (%)					
Alcohol-related	-	1 (17)	3 (50)	2 (50)	0.606
Viral (HBV/HCV)	-	1 (17)	1 (17)	0	0.259
Alcohol-related + MASLD	-	1 (17)	1 (17)	0	0.259
MASLD	-	2 (50)	1 (17)	1 (25)	0.801
cryptogenic	-	0	0	1 (25)	0.202
other	-	1 (17)	0	0	0.411
Data at admission, n (%)					
Ascites	-	5 (83)	5 (83)	4 (100)	0.683
SBP	-	0	0	2 (50)	**0.032**
Other bacterial infection	-	2 (33)	0	0	0.149
Variceal bleeding	-	0	1 (17)	0	0.411
HE	-	1 (17)	2 (33)	1 (25)	0.801
Alcoholic hepatitis		1 (17)	0	1 (25)	0.467
Acute kidney injury	-	0	1 (17)	0	0.411
Laboratory parameters					
Bilirubin, total [mg/dl], median, (range)	-	2.31 (1.3-3.4)	2.14 (1.37-4.60)	3.91 (2.61-5.85)	0.217
AST [U/l], median, (range)		44 (28-64)	61 (35-361)	54 (34-125)	0.294
ALT [U/l], median, (range)		33 (11-38)	32 (17-76)	36 (18-57)	0.709
INR, median, (range)		1.38 (1.20-1.75)	1.46 (1.31-1.77)	1.69 (1.26-2.95)	0.516
Creatinine [mg/dl], median, (range)		0.72 (0.54-0.92)	0.80 (0.60-1.97)	1.36 (1.17-1.62)	**0.012**
Platelets [$x10^3$/L], median (range)		79 (39-176)	75 (41-130)	81 (37-106)	0.972
WBC [$x10^9$/L], median (range)	4.8 (4.0-6.3)	4.1 (2.1-5.7)	5.4 (2.9-7.5)	5.5 (3.4-9.4)	0.476
CRP [mg/L], median (range)	-	16.25 (2.22-76)	13.7 (1.78-45.2)	8.55 (1.23-37.10)	0.567
Severity scores					
Child-Pugh, median, range	-	7.5 (5 - 12)	10 (7 - 11)	11 (8 - 13)	0.126
MELD, median, range	-	12 (8 - 18)	13 (12 - 23)	20 (17 - 27)	**0.033**
CLIF-C AD, median, range	-	47 (41 - 49)	47.5 (41 - 59)	61 (55 - 74)	**0.025**
Treatment at blood draw					
Diuretics, yes, n (%)	-	3 (50)	4 (67)	3 (75)	0.701
Antibiotics, yes, n (%)	-	1 (17)	1 (17)	1 (25)	0.934
Non-selective ß-blockers, yes, n (%)	-	1 (17)	2 (33)	3 (75)	0.169
Albumin, yes, n (%)	-	1 (17)	0	1 (25)	0.467
HE treatment, yes, n (%)	-	1 (17)	3 (50)	3 (75)	0.176
Follow-up and Outcome					

90-day mortality, yes, n (%)	-	0	0	1 (25)	0.229
90-day OLT, yes, n (%)	-	0	0	1 (25)	0.229

HE treatment includes lactulose and rifaximin. Baseline characteristics are depicted as frequencies or median (IQR). Values of *p*-value are based on Wilcoxon–Mann–Whitney test for continuous and chi-square test for categorical variables. *Abbreviations:* SDC, stable decompensated cirrhosis; UDC, unstable decompensated cirrhosis; pre-ACLF, pre-acute-on-chronic liver failure; HBV: Hepatitis B virus; HCV: Hepatitis C virus; MASLD: metabolic-dysfunction associated steatotic liver disease; SBP: spontaneous bacterial peritonitis; HE: hepatic encephalopathy; AST, aspartate aminotransferase; ALT, alanine aminotransferase; WBC: white blood cell count; CRP: C-reactive protein; OLT: orthotopic liver transplantation.